arXiv:0903.2452v1 [astro-ph.EP] 13 Mar 2009

Formation and Detection of Earth Mass Planets around Low Mass Stars

Ryan Montgomery and Gregory Laughlin

University of California Santa Cruz Santa Cruz CA 95064 (U.S.A.)

Number of pages: 32

Number of tables: 2

Number of figures: 8

Preprint submitted to Icarus *13 March 2009*

Proposed Running Head:

Formation and transit detection of terrestrial planets

Please send Editorial Correspondence to:

Ryan Montgomery

UC Santa Cruz Astronomy Department

1156 High Street - ISB 256

Santa Cruz, CA 95064, USA.

Email: rmontgom@ucolick.org

Phone: (831) 459-3809

ABSTRACT

We investigate an *in-situ* formation scenario for Earth-mass terrestrial planets in short-period, potentially habitable orbits around low-mass stars ($M_* < 0.3M_\odot$). We then investigate the feasibility of detecting these Earth-sized planets. We find that such objects can feasibly be detected by a ground-based transit survey if their formation frequency is high and if correlated noise can be controlled to sub-milli-magnitude levels. Our simulations of terrestrial planet formation follow the growth of planetary embryos in an annular region spanning $0.036\,\mathrm{AU} \leq a \leq 0.4\,\mathrm{AU}$ around a fiducial M7 ($0.12M_\odot$) primary. Initial distributions of planetary embryos are calculated using the semi-analytic evolutionary model outlined by Chambers (2006). This model specifies how planetary embryos grow to the stage where the largest embryo masses lie in the $10^{24}g \leq M_{embryo} \leq 5 \times 10^{26}g$ range (corresponding to the close of the so-called oligarchic growth phase). We then model the final phases of terrestrial planet assembly by allowing the embryos to interact with one another via a full N-body integration using the `Mercury` code. The final planetary system configurations produced in the simulations generally consist of 3-5 planets with masses of order $0.1 - 1.0M_\oplus$ in or near the habitable zone of the star. We explore a range of disk masses ($0.2M_\oplus$ to $3.3M_\oplus$) to illuminate the role disk mass plays in our results. With a high occurrence fraction or fortunate alignments, transits by the planet formed in our simulations could be marginally detected with modest telescopes of aperture 1m or smaller around the nearest M-dwarf stars. To obtain a concrete estimate of the detectability of the planets arising in our simulations, we present a detailed Monte-Carlo transit detection simulation incorporating sky observability, local weather, a target list of around 200 nearby M-dwarfs, and a comprehensive photometric noise model. We adopt a baseline 1.5 mmag level of correlated stellar noise sampled from the photometry of the planet-bearing red dwarf Gl 436. With this noise model we find that detection of $1R_\oplus$ planets around the local M-dwarfs is challenging for a ground-based photometric search, but that detection of planets of larger radius is a distinct possibility. The detection of Earth-sized planets is straightforward, however, with an all-sky survey by a low-cost satellite mission. Given a reduced correlated noise level of 0.45 mmag and an intermediate planetary ice-mass fraction of planets orbiting a target list drawn from the nearest late-type M dwarfs, a ground-based photometric search could detect, on average, 0.3 of these planets within two years and another 0.5 over an indefinitely extended search. A space-based photometric search (similar to the TESS mission) should discover ~ 17 of these Earth-sized planets during it's two year survey, with an assumed occurrence fraction of 28%.

Keywords: PLANETARY FORMATION ; EARTH ; TERRESTRIAL PLANETS ; EXTRASOLAR PLANETS ; TRANSIT

1 Introduction

To date, planets have been detected in every region of mass and orbital parameter space to which observational searches are sensitive. In recent years, the minimum detected planetary mass has been decreasing at a very rapid pace. If one projects this trend forward, one sees that detection of the first near Earth-mass extrasolar planets orbiting main sequence stars should occur sometime around 2011. Thus, while it has always been of great interest to search for terrestrial mass planets, the time when success might be obtained now seems close at hand. Indeed, both radial velocity observations and photometric transit surveys have the capability of achieving the detection of Earth-mass planets orbiting nearby low-mass stars. (see e.g. Guedes et al., 2008; Nutzman and Charbonneau, 2008)

In the standard paradigm of Solar system formation, the terrestrial planets emerge during the later stages of proto-planetary disk evolution through the coagulation of smaller bodies (Safronov, 1969) (see Lissauer, 1993, for a detailed review). The initial formation process proceeds rapidly (e.g. Wetherill and Stewart, 1993; Weidenschilling et al., 1997; Kokubo and Ida, 1998, 2000) with a few of the small bodies accreting more matter than their companions, thereby increasing their gravitational cross-sections and experiencing even more rapid growth (e.g. Wetherill and Stewart, 1989) This "runaway growth" phase rapidly produces planetary embryos from the sea of planetesimals. As the embryos grow, they perturb the orbits of local planetesimals, thus reducing gravitational focusing and slowing the continued growth of the planetary embryos. Nevertheless, the largest planetary embryos still accrete material more rapidly than any remaining low-mass planetesimals - leading to the so-called "oligarchic" growth phase. Eventually, an emergent distribution of hundreds of planetary embryos interact and collide stochastically, until all the planetary embryos have either been incorporated into the forming planets or ejected from the system.

N-body simulations of the final accretion phases of terrestrial planet assembly are able to recreate the broad-brush aspects of the inner solar system fairly well (e.g. O'Brien et al., 2006). In particular, the orbital properties of Earth and Venus analogs are often reproduced, whereas Mars-like and Mercury-like objects are harder to account for. Ultimately, however, one would like to test the predictive outcome of the current paradigmatic model on systems other than our own. It has been shown, for example, that initial distributions of lunar-sized embryos similar to the distributions that can generate the solar system terrestrial planets predict Earth-mass worlds orbiting both Alpha Cen A and B (Quintana et al., 2002; Guedes et al., 2008). The accretion of such embryos, however, may be problematic (Thébault et al., 2008, 2009).

Accretion simulations can also be extended to investigate the formation of planets around the low-mass stars that constitute the bulk of the local stellar population. For example, Raymond et al. (2007) present a suite of accretion calculations which predict that Earth-sized terrestrial planets should be rare around M-type stars with $M_* \lesssim 0.3M_\odot$. Their models start with initial planetesimal surface densities that scale generally downward from the minimum mass solar nebula-based models studied by Chambers (2001). Indeed, the Raymond et al. (2007) result can be encapsulated by stating that low-mass planetesimal disks produce low-mass planets. Their work makes it clear that if the protoplanetary disks associated with the lowest mass stars are scaled down versions of the Sun's protoplanetary disks, then habitable planets orbiting red-dwarfs will be very rare. The Raymond et al. result emphasizes the importance of observations probing inner disk masses as the available mass in these regions is pivotal to the formation of habitable planets *in-situ*.

Planetary formation around M-dwarfs is now the focus of considerable observational and theoretical work. One conclusion that seems robust is that Jovian-mass gas giant planets around M-dwarfs should be rare if outer disk masses scale with stellar mass (e.g. Laughlin et al., 2004). This prediction is a natural consequence of the core accretion theory for giant planets (see, e.g. Pollack et al., 1996; Hubickyj et al., 2005), and now has supported from observations (Butler et al., 2004; Endl et al., 2006; Lovis et al., 2006). Furthermore, ice-giant planets akin to Uranus and Neptune should be common around M dwarfs. This result is lent plausibility by the radial velocity observations of Mayor et al. (2008) who estimate the fraction of FGK stars with ice-giant planets to be at least 30%, and by microlensing results (e.g. Bennett, 2009) which give direct evidence of such planets. Since accretion models are so dependent on the available mass, the seeming plethora of planets is hard to understand if the only available initial condition is a scaled version of the MMSN. Thus, because M stars allow for ready detection of companions down into the terrestrial mass range, we think it is of interest to investigate the observable consequences of a broad range of possible formation scenarios.

The plan for this paper is as follows. In §2, we describe the details of our terrestrial planet formation model for low-mass stars. This model is designed from the outset to favor the production of habitable planets orbiting red dwarfs. In §3, we describe the specific simulation outcomes for our model, and aggregate their statistical properties. In §4, we construct end-to-end Monte-Carlo simulations that realistically assess the near-term prospects for finding these planets using inexpensive photometric surveys that target nearby stars. In §5, we conclude with our finding that a ground-based survey with small dedicated telescopes has difficulty providing significant constraints on our scenario, but that an inexpensive microsatellite survey can provide a significant test.

2 Formation Simulation Method

We have carried out 40 N-body accretion simulations of terrestrial planet formation around low mass stars. The simulations use initial conditions that are generated with a semi-analytic model that is very similar to that described in Chambers (2006). The semi-analytic evolutionary model is intended to encapsulate the growth of bodies up to and including the oligarchic growth phase, and includes (1) a disk of equal-mass planetesimals with their equilibrium eccentricities and inclinations, (2) a gas disk which acts to damp these eccentricities and inclinations, and (3) seed planetary embryos which accrete material throughout the simulation and dynamically heat the planetesimal distribution. As the planetary embryos grow, they accrete and retain atmospheres, which increase their collisional cross-sections, and further accelerate their growth. A semi-analytic evolution is deemed complete when the distribution of bodies in the model reaches 50 planetary embryos (each separated by 10 mutual Hill Radii). At this point the mass in planetary embryos and planetesimals is approximately equal ($\sim 1.6 M_{\oplus}$ in each population), and we take the orbital parameters of the embryos and the surface density profile of the remaining planetesimals and fragments as the initial condition and transfer the system to a 3 dimensional N-body simulation. Our N-body simulations begin with the 50 planetary embryos and include 50 additional particles as representatives of the remnant planetesimal population. Because we begin with equal numbers, the masses of the 'super-planetesimals' and the planetary-embryos are approximately equal (although as the simulations proceed, the embryos rapidly outpace the planetesimals).

The bodies orbit a late type M-dwarf star (M7, $M_\star = 0.12\ M_\odot$) and are endowed with random orbital eccentricities in the range $[0.00 < e_i < 0.01]$, and random orbital inclinations in the range $[-0.5^\circ < i_i < 0.5^\circ]$. The initial longitudes of periastron, ϖ_i, longitudes of the ascending nodes, Ω_i, and mean anomalies, M_i, of the bodies are chosen randomly.

Due to the uncertainties in the surface density profile and to facilitate comparison with previous work, our semi-analytic model draws on an initial solid surface density profile chosen to resemble the Minimum Mass Solar Nebula (Weidenschilling, 1977) in that it falls as $\Sigma = \sigma_0 \cdot (a/1\,\mathrm{AU})^{-3/2}$ until it reaches the 150 K ice-sublimation temperature (Podolak and Zucker, 2004) where we truncate the outer edge of the disk. This choice of surface density profile plays a significant role in our investigation - given a shallower profile, formation of terrestrial planets in M-dwarf habitable zones *in-situ* becomes more difficult (Raymond et al., 2007), and under these conditions, the smaller planetary population would be undetectable given current ground-based photometric precision. In our model, spurred on the results of Mayor et al. (2008) and Bennett (2009) we imagine that an ice-rich (and up to Neptune-mass) object has already formed in the region exterior to the ice-line due to the larger initial solid surface densities there (in analogy with the formation of Jupiter prior to the formation of the Earth). Given our fiducial luminosity $L_* = 0.02L_\odot$, the 150 K fiducial ice-line lies at $r_{150K} = 2.7\,\mathrm{AU}\sqrt{\mathrm{L_*/L_\odot}} = 0.4\,\mathrm{AU}$. We note that this is only an approximate boundary. In order to account for the destructive nature of collisions in the inner regions (where collisional speeds are faster) we truncate the inner edge of the disk by taking Chambers' (2001) inner disk Keplerian cutoff velocity: $v = 54\,\mathrm{km/s}$ at $r_{in} = 0.3\,\mathrm{AU}$. Around our low-mass primary ($M_* = 0.12 M_\odot$) this velocity sets the inner edge of the disk to $r_{inner} = 0.036\,\mathrm{AU}$.

The value of σ_0 for the minimum mass solar nebula is $\sigma_{0,MMSN} = 7\,\mathrm{g/cm^2}$. Raymond et al. (2007) show unambiguously that when the MMSN is extrapolated to lower disk masses, the resulting terrestrial planets rarely exceed the mass of Mars. We thus ask: is there any evidence beyond the MMSN to which we can look that might suggest higher surface density normalizations for the disks orbiting the lowest mass stars?

Sub-millimeter flux measurements of low-mass primary systems (e.g. Andrews and Williams, 2007) suggest a possible linear correlation between stellar-mass and disk-mass for low-mass stars, albeit with a large amount of scatter. To quantify this effect, we calculate occurrence fractions of Earth-mass or larger circumstellar disks given a mean solar type disk-mass of $0.005 M_\odot \pm 0.5 dex$ and scaling down to our stars' disk masses by assuming that the disk-mass scales with the stellar-mass to the 0th, 1st or 2nd power. For these three scaling possibilities (0, 1, 2) we find occurrence fractions of (28%, 0.7%, 0.001%), respectively. Further, there is a scatter of around an order of magnitude on either side of the MMSN value of $M_{disk} \sim 0.01 M_\odot$ for a given stellar-mass primary. This serves to restrict the likely surface-density normalization to between 0.1 and 10 times the MMSN value of $\sigma_{0,MMSN} = 7\,\mathrm{g/cm^2}$.

Searching further afield, we can draw clues from other satellite systems orbiting primaries other than the Sun. First, consider the Jovian satellite Io: Jupiter's mass is $0.001 M_\odot$ and Io, with $P = 1.8$ d, has $M = 8.93 \times 10^{25}\,\mathrm{g}$. If we spread Io's mass out following the $r^{-3/2}$ surface density profile, we find $\Sigma \sim 11,000\,\mathrm{g/cm^2}$ at Io's orbital radius. Next, consider the GJ 876 system, with $M_* = 0.32 M_\odot$ (Rivera et al., 2005). Planet 'd' has a $P = 2$ day orbit ($a = 0.02\,\mathrm{AU}$) and $M = 7.5 M_\oplus$. If one assumes that planet d formed from material extending to $r \sim 0.075\,\mathrm{AU}$ and if this material is distributed as $\Sigma \propto a^{-3/2}$, then we again find $\Sigma \sim 1.1 \times 10^4\,\mathrm{g/cm^2}$ at the $P = 2$ d orbital radius.

Going out on a limb, one could argue that this similarity between Io and GJ 876 d implies that low-mass primaries can have $\Sigma \sim 1.1 \times 10^4\,\mathrm{g/cm^2}$ at the 2-day orbital radius. We adopt this surface density normalization in our simulations. Certainly, such an assumption is, at this point, mere conjecture, but by the same token, a large downward extrapolation from the MMSN seems equally uncertain. In our model, if we extrapolate to 1 AU, one finds $\sigma_0 = 21\,\mathrm{g/cm^2}$. This value, while high, does fall within the large range of acceptable surface densities inferred from the extant sub-millimeter data.

Canup and Ward (2006) have noted the striking similarity in mass ratios between the Jovian planets (Jupiter, Saturn, Uranus) and their regular satellite systems: $m_s/M_p \sim 2 \times 10^{-4}$. They suggest that this points to a common formation scenario within gas-starved circumplanetary disks. In our red dwarf context, the presence of an exterior ice-giant planet may play a similar role. A Neptune-mass planet orbiting a $0.1 M_\odot$ primary at these radii could meter the inward flow of gas through the gap that it has opened in the protoplanetary disk. The details of the inflow are dependent on the details of the gas flow around the co-rotational resonances and so is largely undetermined for the present situation. We hypothesize that the slow metering of gas into the inner region allows planetesimals to build up without suffering the catastrophic effects of Type I migration Canup and Ward (2006). This would lead to a reduced gas-density in the interior orbital regions which would significantly reduce the effect of Type I migration. In the present work we make the assumption that such a mechanism makes the effects of Type I migration negligible over the planet mass range studied, but we have not done a detailed analysis and this scenario would definitely require further investigation should observations reveal the presence of a terrestrial-mass planetary population orbiting nearby M dwarfs.

Terrestrial planets that form in a mode analogous to Jovian satellites would be expected to be relatively volatile-poor, while volatile-rich planets (which would have larger radii at a given mass) would be indicative of a planet that migrated inward rather than forming *in-situ* (Gaidos et al., 2007; Raymond et al., 2008). The lowest-mass M dwarf target stars are nearby, and so follow-up radial velocity measurements are possible (Bouchy et al., 2005). An Earth mass planet in a 30 day orbit around our fiducial $0.12M_\odot$ star would elicit a radial velocity half-amplitude of $K = 0.85$m/s and so is detectable given current technology (Lovis et al., 2008). Measurement of the Doppler wobble generates a mass, and when combined with the radius from the transit photometry could distinguish between the two scenarios. (This situation could, of course, be complicated by the presence of significant gas atmospheres augmenting the planetary radii Adams et al. (e.g. 2008)). Assuming similar volatile distributions to solar-type stars, it seems likely that water content levels on these planets would be similar to those predicted by Raymond et al. (2004). However, for the purposes of probing bulk composition, transits can only make zeroth-order comparisons. It is interesting to speculate as to the water content of these terrestrial planets but, as yet, the situation is largely unconstrained.

Given these considerations, we set the initial solid surface density around our M7 star to be $\Sigma = 21 \times \left(\frac{a}{1\,\mathrm{AU}}\right)^{-1.5}$ g/cm^2, where almost all of this mass is in the form of a population of 5 km (10^{18} g) planetesimals. The disk scale-height is $H = 0.05\left(\frac{a}{1\,\mathrm{AU}}\right)^{1.25}$ AU. We adopt constant-mass planetesimals, in keeping with Chambers (2006). This assumption greatly simplifies the semi-analytic framework with the drawback of possibly introducing a modest overestimation of the embryo growth rates. The remainder of the solid surface density (0.03% by mass) is allotted to planetary embryos in accordance with the constraint, derived by Ida and Makino (1993), that the onset of oligarchic growth occurs when the embryo and planetesimal masses and surface-densities satisfy $2M_{emb}\Sigma_{emb} = m_p\Sigma_p$. We set the average inter-embryo spacing to be 10 R_{Hill} in keeping with Kokubo and Ida (1996). We also include a gas disk which serves to damp the planetesimal's eccentricities and inclinations and causes the planetesimals to drift inwards via gas drag. We implement the effects of gas drag using the prescription of Adachi et al. (1976). The gas disk begins with an initial surface density of 200 times the solid surface density and, over the course of the simulation, the gas dissipates according to $\Sigma_{gas}(t) = \Sigma_{gas}(0)\exp(-t/\tau_{neb})$, where $\tau_{neb} = 2\,\mathrm{Myr}$.

As the random velocities of the planetesimals rise, collisions between planetesimals will become destructive, giving rise to many small collision fragments. Because these fragments are so small, the gas is very effective at damping out the eccentricities and inclinations of these fragments. Thus we treat this population as having zero eccentricities and inclinations. This greatly strengthens gravitational focusing between the embryos and the fragments, thereby increasing the growth rate of embryos substantially over what would occur without fragmentation. We also include the effects of the embryo's nascent planetary atmospheres. This also tends to increase the embryo's collisional cross-sections, further increasing the growth-rates. With all of these factors included we find that our embyro growth-rates are a few (~ 3) times faster than the equilibrium-regime approximation of Chambers (2006) (eqn. 6), and ~ 8 times faster than the estimation given by Kokubo and Ida (2002) (eqn. 15).

We run the semi-analytic model until it produces 50 planetary embryos separated by 10 Hill Radii (at which time the embryos have grown to sizes between 1×10^{24} and 5×10^{26} grams). We then replace the remaining planetesimal surface distribution with 50 "super-planetesimals" (each with $m_p \simeq 2 \times 10^{26}\,\mathrm{g}$). The 50 embryos and the 50 super-planetesimals are evolved using the `Mercury` integrator package (Chambers and Migliorini, 1997) which employs a hybrid algorithm that integrates the bodies with a symplectic map and switches to Bulirsh-Stoer integration when close encounters occur. In this new framework, the embryos are self-gravitating while the super-planetesimals are not. Each N-body simulation is run for 100 Myr to help ensure the long term stability of the emergent systems. The hybrid integrator uses a variable stepsize to meet a Bulirsch-Stoer step-wise error tolerance of 10^{-12}. The typical energy error at the end of one of our integrations is $\sim 4 \cdot 10^{-4}$.

In order to address the uncertainty in the disk mass used we have run simulations with different disk surface-density normalizations. If the total disk-mass scales as the stellar mass as is implied by Andrews and Williams (2007) and if the disk surface density normalization in our region scales as the total disk-mass, then the mean normalization for the disk surface-density, $\sigma_0 \sim 7\,\mathrm{g/cm^2} \times 0.12 = 0.84\,\mathrm{g/cm^2}$. The resulting inner disk would only contain $0.17 M_\oplus$ and thus cannot host detectable terrestrial planets formed *in situ*. In order to quantify this situation, we have performed simulations of planetary formation and detection with normalizations of $\sigma_0 = 0.84\,\mathrm{g/cm^2}$ and $\sigma_0 = 7\,\mathrm{g/cm^2}$. The resulting detection statistics are low to zero, as expected, and are presented for completeness in Table 2.

3 Formation Simulation Results

Our semi-analytic model seeks to simulate the final, rapid, stages of oligarchic growth that follow the runaway growth phase. Initial planetary embryo masses are $M_{emb} \sim 3 \times 10^{21}$ g. The semi-analytic model allows the planetary embryos to achieve presumably more natural mass and spatial distributions, leading to a more robust set of initial conditions for the final, stochastic, phase of growth. In Fig. 1, the thin and thick lines represent beginning and end states of the semi-analytic phase of the simulation. The solid surface density begins almost entirely in the form of planetesimals and after 100 years of growth, the inner region has become dominated by the planetary embryos. At this point, the planetary embryos are large enough that, maintaining the average inter-embryo spacing suggested by Kokubo and Ida (1998), the surface density profile can support 50 such embryos. Using simple time scale analysis, we can compare this oligarchic growth rate with other calculations. We find that τ_{grow} obtained at $a = 0.1\,\mathrm{AU}$ around our M7 dwarf is 29 times shorter than that found in simulations designed to mimic the solar system at $a = 1\,\mathrm{AU}$ (Chambers, 2006). Given the approximate nature of timescales, this is consistent with the acceleration to be expected (see §3.3 for a detailed calculation).

Once the semi-analytic model has generated initial conditions, we transfer the remaining planetary embryos to the N-body simulations. At this transition, the gas is suddenly removed. Figures 2 and 3 show the evolution of two of the simulations, one from Group A (with nothing exterior to the ice-line), and one from Group B (with a Neptune-mass body on a 0.6 AU nearly circular orbit). The sizes of each of the symbols are proportional to the radius of the body.

Figure 2 shows the evolution of simulation A-01. After 3,000 years, mutual interactions have slightly increased the eccentricities of the bodies, and we see the rapid buildup into protoplanets of approximately Mars-mass. By 0.1 Myr, we see the formation of a few bodies with $M_{embryo} \simeq 0.7 M_{\oplus}$, predominantly in the innermost regions of the disk where the surface density is high and where the timescales are short. These massive embryos rapidly clear out the surrounding regions of lower mass planetary embryos through collisions and scattering. Over a timescale of order $\tau \sim 1$ Myr, these larger bodies slowly scatter or accrete the remaining planetary embryos. Finally, those larger remaining bodies settle into low eccentricity orbits through the ejection or accretion of the remaining smaller planetary embryos, producing a system of planets with masses between Mars' and Earth's. These remaining planets are in low eccentricity orbits separated by, on average, 30 mutual Hill radii. Thus, while long term stability is not assured for these systems, it is quite likely for extremely long timescales (Chambers et al., 1996).

Figure 3 shows the evolution of simulation B-01. (the Group B simulations included a Neptune-mass planet at 0.6 AU) The external perturber's influence is noticeable early on through the excitation of eccentricities of several planetary embryos around the 2:1 resonance at 0.378 AU as well as the increased eccentricities of the entire population relative to that seen in the early evolution of simulation A-01 (Fig. 2). The orbits rapidly become excited due to mutual interactions amongst themselves and the perturber, resulting in a dynamically warm system. Within approximately 10,000 years, the system has built up a handful of Mars-mass planets through collisions between the planetary embryos. The growth rate then slows considerably and over the later stages of the disk's evolution the larger surviving planets eject most of the other remaining low mass bodies with the help of the massive perturber. The surviving planets are on low-eccentricity orbits which are separated by, on average, 17 mutual Hill radii. The overall situation is similar to that of Group A: the planetary embryos have been efficiently ejected or accreted onto the remaining planetary bodies which are between Mars' and Earth's mass and whose orbits are located from the star's habitable zone outwards.

An accretion timescale of 10,000 years seems surprisingly short, but it is nevertheless a natural consequence of the fact that the growth rate scales as $\tau_{growth} \propto v \cdot \rho^2$. Although our region of interest ($a \simeq 0.1\,\mathrm{AU}$) is close to the primary, the star is also less massive ($M_* = 0.12 M_\odot$) resulting in very similar orbital velocities to the solar system ($v \simeq 1.1 v_\oplus$). For this planet-forming region we can compare the local density to the solar system; $\rho/\rho_{MMSN} = 4.67$, giving our growth timescale relative to the solar system as: $\tau_{growth}/\tau_\oplus \simeq 24$. Thus our simulations after 100,000 years of evolution should look similar to simulations done of the solar system at approximately 2.4 million years (Chambers, 2001). This is indeed the case.

Considering planets that exceed the mass of Mars by the end of our simulations, we see that their mass accretion is 50% complete at $\tau_{50} = 8 \times 10^4$ yr and 90% complete at $\tau_{90} = 10^6$ yr. The rapid initial evolution arises from the initial flurry of accretion activity in the dense environments. The presence of an external perturber accelerates this timescale significantly: the 50% and 90% stages are reached at median times of $\tau_{50} = 2 \times 10^4$ yr and $\tau_{90} = 0.2 \times 10^6$ yr, respectively.

With 20 complete simulations in both groups A and B, we can consider the statistics of our systems. Figure 4 shows the resulting histogram of the planetary masses. The two distributions are roughly similar over most of the mass range, implying a concordance in the average number and masses of planets. At the lowest masses, however, we see the primary effect of an external perturber on the surviving populations. The ice-giant is very efficient at ejecting low mass planetary embryos, thus the final planetary mass distribution of Group B is made up of a population which is distributed around $0.7 M_{\oplus}$. In addition, Group A has a low-mass remnant population that survived with few if any collisions and only mild scattering events. We wish to isolate the general properties of the two distinct populations of surviving bodies. We thus draw a division between the two at $0.05 M_{\oplus}$. The resulting averaged quantities of interest are presented in Table 1. The effect of inclusion of an ice-giant is that it serves to raise eccentricities of the low-mass planetary embryos from the simulations leading to ejection or accretion onto the star. This decreases the average planetary mass slightly, and also limits the growth of the remaining planets to the inner disk regions. Previous work that compared terrestrial planet formation with and without giant planets (Levison and Agnor, 2003) found that when giant planets caused significant mass-loss from the system the resulting terrestrial planets tended to be smaller and closer in to their host stars. This is consistent with our findings: when the ice-giant was included we have significant mass-loss and find that our resulting planets are smaller and closer in to the star. Figure 5 shows the mass found in each bin of semi-major axis for Groups A and B. Note that the majority of the massive planets are located inside or very close to the star's so-called habitable zone ($0.03 - 0.08\,\mathrm{AU}$) (Selsis et al., 2007). In any case, planetary habitability depends on a variety of factors, and in general can only be evaluated once the precise orbit, stellar environment and bulk structure of a given candidate have been determined.

4 Detection Simulation

Our simulations create potentially detectable planets. Our formation scenario is therefore testable, since a M7 ($\sim 0.145 R_\odot$) primary presents a generous 0.4% transit depth for a terrestrial ($\sim 1 R_\oplus$) planet. Furthermore, habitable planets orbiting such stars enjoy a relatively high a-priori transit probabilities in comparison to an Earth-analog orbiting a solar type star. The a-priori geometric transit probability for a habitable planet emerging from our simulations is of order

$$P_{transit} \simeq 0.0045 \, \frac{1\,\mathrm{AU}}{a} \left(\frac{R_\star + R_p}{R_\odot} \right) \frac{1 + e\cos(\pi/2 - \varpi)}{1 - e^2} \simeq 1\%, \tag{1}$$

where ϖ is the longitude of periastron referenced to the plane of the sky, and the other symbols have their usual meanings.

Given a transit depth and a specified detection strategy, we can compute the detectability of our model planets. Figure 6 shows the average detection probability per stellar system observed as a function of detection sensitivity threshold. For example, if the noise can be controlled to allow the detection of planets generating central transit depths deeper than 0.4%, then each planet-bearing star yields a $P \sim 3.2\%$ chance of a detection. The situation thus looks promising. Unfortunately, however, the photometric variability of late-type M-dwarfs complicates detection and requires us to carry out a more realistic appraisal of the detectability of the planets that form in our simulations.

Fully convective stars near the bottom of the main sequence often display significant magnetospheric activity and accompanying photometric variability (Rockenfeller et al., 2006). This is demonstrated by the variability of M-dwarfs, e.g. Proxima Centauri, which exhibits X-ray flare activity with possible attendant photometric variation. In general, this variability can be modeled as longer-period correlated or "red" noise. Red noise levels in these stars slows the noise attenuation of phase-folded photometry from $1/\sqrt{N_{data}}$ to $\sim 1/\sqrt{N_{transits}}$ (Pont et al., 2006). The half-life of the red noise in this approximation is four times the transit periodicity (days to years) rather than four times the photometric cadence (seconds to minutes). Due to this extremely slow error convergence, the utility of rapidly taking multiple exposures is greatly reduced. It is thus likely that a successful observational campaign will need to attain cadence and signal-to-noise levels that allow the detection of a transit to high confidence on the basis of a single event. The candidate transit then triggers a relatively intense follow-up campaign that ideally begins while the initial event is in progress. The *MEarth* survey described in Nutzman and Charbonneau (2008) provides an example of this type of detection strategy and the calculations that follow are based on their scenario.

Our approach requires an estimate of stellar photometric noise over a time scale of hours. As a concrete example, we take our noise model from photometric observations of GJ 436 (Gillon et al., 2007) as obtained using the Wise 1m telescope on April 24th, 2007. This data set illustrates, to a first approximation, the sort of data that might be regularly obtained by a ground-based survey using dedicated small telescopes. The Gillon et al. photometry was obtained during an 2.9-hour observation centered on the transit of Gliese 436 b. Adopting only the photometry outside of transit yields 177 photometric points over 2.12 hours with a standard deviation of 0.39%. No previous treatment has been applied to the data aside from the standard reduction and differential photometry. We process this data to produce a photometric red noise signal that can be applied to generate Monte-Carlo data as follows.

First, we distribute the Gillon et al. (2007) photometric data into 10-minute bins, and use the photometric scatter within these bins to calibrate a model for the white noise contribution. We generate synthetic 177-point datasets of pure Gaussian noise and calculate the standard-deviation within bins of 14 data points. We repeat this procedure until the restricted standard-deviation converges and the difference from the known noise amplitude supplies our correction factor for the white-noise amplitude giving $\sigma_{white} = 0.36\%$. We then use the Scargle periodogram of the remaining longer-period noise (the smoothed photometry) at periods from 10 minutes to 12 hours to generate synthetic 177-point datasets. We sum one hundred cosines of random phases with the amplitudes given by the periodogram to the white-noise. We then iteratively adjust the amplitude of the long-period noise until the overall noise amplitude of the synthetic datasets converges to that of the Gillon et al. (2007) photometry.

Our estimate of the longer-period red noise, $\sigma_{red} = 0.15\%$, is intended to be independent of the noise introduced by the telescope and is assumed to arise from intrinsic stellar variability on short timescales. Red noise will limit the sizes, and hence the masses of the planets to which our observational campaign is sensitive. A search strategy that forgoes folding must be able to detect a transit with sufficient signal-to-noise to minimize false-alarms and expensive large-telescope follow-up to an acceptable level. Thus, even with zero white-noise, we are limited to stars that are small enough to show a transit from one of our planets that rises significantly above the red noise level. For example, if we demand 4σ confidence in the reality of a given transit signal, we could survey only stars small enough to yield transit depths of at least $\sim 0.6\%$. The red noise amplitude will vary with time, and from star to star. Hence the estimate of $\sigma_{red} = 0.15\%$ adopted here should be understood to provide only a starting point for a more detailed investigation.

Obviously, our strategy benefits from a ready supply of small nearby stars. To quantify the available census, we adopt the Lépine-Shara Proper Motion Catalog - North (Lépine and Shara, 2005). We begin with the local subsample of the proper motion catalog (Lépine, 2005) consisting of 4131 dwarfs, subgiants and giants located within 33pc of the Sun. Following the lead of Nutzman and Charbonneau (2008), we use color cuts to restrict the list to 2401 local M-dwarfs by requiring that $H-K < 0.7$, $J-H > 0.12$, $J-K > 0.7$, and $8 < H < 15$. We estimate the stellar mass using the Delfosse et al. (2000) mass-luminosity relation and then we use the Bayless and Orosz (2006) empirical mass-radius relation to approximate the stellar radii. Given the stellar radii, we further restrict the sample to harbor only stars with radii small enough to allow detectable transit depths (above a threshold of $TD_{crit} = 4\sigma = 0.6\%$). We thus adopt a transiting planetary radius of $1.2R_{\oplus}$, and require this size planet's transit signal to be equal to or greater than TD_{crit}. This adopted planetary radius is chosen so that we will only exclude from our target lists those stars which are so large that detection of any of our formed planets is unlikely. In effect, this restricts our target list to only those late-type M-dwarfs of radius $R_{*} \simeq 0.12R_{\odot}$. This profoundly limits the sample, leaving a prime catalog of 169 local, very late-type M-dwarfs. These stars offer the single best opportunity to detect a habitable transiting planet from the ground.

We need to monitor M dwarfs with repeated visits at a cadence that is slightly more frequent than the expected transit duration. We must therefore evaluate the signal-to-noise levels for any star-telescope combination as a function of integration time. Following Nutzman and Charbonneau (2008) we use the bolometric corrections of Leggett et al. (2000) to derive the stellar luminosities. Luminosities and radii yield values of the stellar effective temperatures, T_{eff}. Our mass and radii estimates then provide surface gravity ($\log g$) estimates for our stars. With T_{eff} and $\log g$, we can specify a synthetic stellar spectra, $f(\lambda)$ (Hauschildt et al., 1999). When combined with a target's distance, d, this synthetic spectra provides an estimate of the incident stellar flux

$$F(\lambda) = f(\lambda)\left(\frac{R_*}{d}\right)^2 \frac{\lambda}{hc}, \tag{2}$$

where $F(\lambda)$ has units of photons/cm^2/sec/Å. With these assumptions, the number of photons received, N_{ph}, from a given target in exposure of length t on a telescope of diameter D, is

$$N_S ph = t \times \pi(D/2)^2 \times \int F(\lambda)T(\lambda)\mathrm{d}\lambda\ , \tag{3}$$

where $T(\lambda)$ is the telescope's transmission function. Our transmission function mimics Nutzman and Charbonneau (2008) 'i+z' filter that opens at around 700nm and stays open for longer wavelengths, combined with the quantum efficiency of a typical commercially available CCD (which falls redward of 800nm and completely closes off by 1000nm). We enforce an additional throughput loss of 50% to account for other unaddressed potential effects.

With a photon count, we can obtain an accurate estimate of the photometric signal produced by a given target. We approximate the signal-to-noise ratio of an exposure as:

$$SNR = \frac{N_{ph}}{\sqrt{N_{ph} + N_{ph}^2(\sigma_{scint}^2 + \sigma_{red}^2) + n_{pix}(N_{sky}t_{obs} + N_{dark}t_{obs} + N_{read}^2)}} \tag{4}$$

where $\sigma_{red} = 0.15\%$ as stated above, and σ_{scint} is given by the scintillation expression of Dravins et al. (1998). The quantity n_{pix} represents the expected number of pixels covered by the stellar image. $N_{sky} = 10^{-5}\,\mathrm{e^{-}pixel^{-1}sec^{-1}}$ is an estimate for the sky brightness. $N_{dark} = 1.4 \cdot 10^{-4}\,\mathrm{e^{-}pixel^{-1}sec^{-1}}$ is an estimate of the dark-current noise based on the Nickel 1-meter telescope's direct imaging camera CCD at Mount Hamilton. $N_{read} = 11.7\,\mathrm{e^{-}pixel^{-1}}$ is the amplifier-generated readout noise, again based on the Nickel 1-meter's CCD specifications. For reasonable ground-based exposure times the readout noise dominates over the dark-current and sky, contributing $\sim$ 0.4 mmag noise. Thus, for red noise levels below 0.4 mmag the readout noise of our camera will begin to dominate the SNR value. For fixed telescope size and exposure time, the required SNR yields a tradeoff between spurious transit-like noise and missed transits. Our goal is to optimize the choices of telescope diameter, exposure time, and SNR value for recovery of our simulated planetary population. Our exposures must be a few times shorter than the expected transit duration. For close-in terrestrial planets whose transit durations are less than 60 minutes, this limits the exposure time to less than about 20 minutes. Given this maximum exposure time, we can estimate $N \sim 21$ observations per 7-hour night. Three targets on a given night yields $\sim$ 7 photometric observations per star. We thus also require that noise be discernible from a transit signal at the 4.3σ level, allowing $\sim$ 99.8% confidence in any given ($\sim$ 7 point) lightcurve. We adopt telescope sizes of 1 meter in keeping a realistic expectable financial investment for a dedicated array.

Figure 7 shows the number of stars that are bright enough to allow observation within 20-30 minute exposures for varying stringencies of the required SNR. Note that there are few stars which allow a statistically significant detection. For example, if we adopt a detection criterion of 3σ, the number of available target stars is unacceptably low ($\sim$ 10). Thus, for correlated noise levels $\sigma_{red} \sim 0.15\%$, the prospect of detecting transiting Earth-sized planets with an array of meter-class ground based telescopes is challenging. Our Monte-Carlo detection simulations therefore examine the effects of different levels of correlated noise.

Our observability simulations extend the work of Seagroves et al. (2003) and specific details of the computational procedure can be found in that work. A Monte Carlo simulation is initialized with the planetary populations (drawn from our simulations), a list of observers, and a stellar target list (the low-mass stars defined by $TD > TD_{crit}$). Each observer has an associated location (latitude, longitude and altitude) and weather (average fraction of clear/cloudy nights per year). Each target has an associated position (R.A. and Dec.), stellar mass, and a photon flux over the wavelength region of interest. The Monte Carlo routine starts by assigning which targets will host transiting planets in the simulation. The program assigns planetary systems (the end-state of our N-body simulations) to a fraction of these target stars and then orients those planetary systems randomly with respect to the line-of-sight to Earth. Assigned planets maintain their orbital periods, and hence assume a semi-major axis in concordance with the parent star mass and Kepler's third law. The simulation proceeds through an observing campaign night by night. Every night, the simulation must determine where the weather is favorable: while season-based weather patterns have not been figured into the model, the fraction of clear and cloudy nights at each observing location is known[1]. The night's weather for each location is determined by drawing from these probabilities. If clear or cloudy, all observers common to the location will be affected identically. If the weather is determined to be partly cloudy in a given location, then it is possible that some observers at that location will be able to observe while others will not. For each observer at a location with favorable weather, the Julian dates (JD) of sunrise and sunset at the observer's location are calculated for the current date in the campaign. The JD of sunset, the position of each target, and the observer's location are used to calculate air masses for each target in the target list. Any targets that pass the airmass cutoff ($\sec(z) = 2.5$ in our simulations) at sunset are then checked to ensure they will pass the airmass limit for at least 2 hr. Each observer will then construct a target-list from those targets that have passed the airmass cutoffs and whose required exposure times are short enough to allow multiple targets to be observed every hour. The observer then cycles through this observing list every hour until one of the targets fails an airmass test, at which point it is dropped and a new target is added to the observing list. On each visit, an observer integrates long enough to reach a 5σ signal-to-noise ratio before slewing to the next target (1 minute of combined slew and readout time is added between each target in the observing schedule). This level of signal-to-noise is higher than that used to signal a detection so that we are able to detect transits more quickly and reliably. Once a detection has been made, we anticipate extensive follow up observations by larger telescopes, however in this preliminary study we do not modify our observing plan as a result of transit detections. The list is repeated every hour so as to catch the majority of transits that might occur over the course of the night. In the event that one of the targets hosts planets, and that one of the planets happens to transit during the night's observations, the line-of-sight separation between the planet and its host star is calculated. Using this separation, as well as the radii of the transiting planet and its host star, the photometric transit depth is determined using the approximate formulae of Ohta et al. (2005). This process is repeated for each observer in the observer list, and the aggregate process constitutes 1 night of the campaign.

---

[1] http://www.ncdc.noaa.gov/oa/climate/online/ccd/cldy.html

The simulation then increments its internal calendar by 1 day and repeats the procedure for the overall duration of the campaign. Using this rotating observation method rather than continual monitoring of individual targets allows us to monitor several stars simultaneously with only minimal loss of coverage: the typical transit length is one hour, so one observation every hour should catch any transits that occur. In comparison, the typical orbital period is between 10 and 60 days, so if we wished to monitor individual stars continually we should do it at least over this time range. This severely limits the rate at which we could study our targets, extending the necessary time to discovery by many years.

The results of the Monte-Carlo simulation depend on the number and distribution of observers, the stringency of the detection criterion (SNR-value), and the adopted level of correlated noise. We set the fraction of stars with planets to 100%, this result is of course downwardly scalable. As an illustrative case of a viable search strategy, we distribute 10 observers in longitude around the Northern hemisphere. We choose this distribution of observer locations envisioning the utilization of a pre-existing infrastructure of small telescope observers (Seagroves et al., 2003), and we note that such a distribution could be altered more observers at fewer sites without a significant impact on the cadence or quality of the results. We choose this distribution of observer locations envisioning the utilization of a pre-existing infrastructure of small telescope observers (Seagroves et al., 2003), and we note that such a distribution could be altered more observers at fewer sites without a significant impact on the cadence or quality of the results. Each observer operates a 1-meter telescope and signals a potential transit whenever a photometric measurement falls 4.3σ below the night's average. This stringent detection criterion of 4.3σ was chosen to reduce false-positive occurrence to acceptable levels. Due to the highly non-Gaussian nature of the false-positive rate, we iterated to determine this optimal value of 4.3σ where we were able to reduce the false-positive rate to (on average) 19 over the entire two-year campaign while still allowing reasonable integration times. We vary the amplitude of the correlated red noise from 1.5 mmag to zero, and for each red noise level we repeat the model observing procedure several (5-10) times. The averaged results stemming from 135 Monte-Carlo simulations are presented in Fig. 8. A ground-based transit search of the above specifications is able to detect Earth-sized planets with acceptable levels of false-positives when red noise is controlled to the level of 0.45 mmag (30% of the adopted value). Over the course of a two year campaign the observers produce approximately 9000 photometric light-curves. Of these light-curves, on average 5.5 contained true transits and 1.3 of these were detected at the reduced level of correlated noise (0.45 mmag). At the end of these campaigns there are another 1.5 transiting planets that could be detected but haven't yet, thus a campaign that utilized more observers or an extended search would be expected to detect a total of ~ 2.8 transiting planets given the reduced level of red noise. If we utilize the $h = 0$ scaling occurrence fraction of $f = 28\%$. We obtain an estimate of 0.8 detections. Our results are tabulated based on planetary radii drawn from the results of Valencia et al. (2007) that assume ice-mass fractions of 0%, 50%, and 100%. This allows us to cover a reasonably expected range of possible planet compositions and sizes, the resulting planetary radii, number of planets detected under said observing campaign and the number of potentially detectable planets under this observing configuration are presented in Table 2. These other simulated observing campaigns are only different in the planetary radii used, all other parameters were held constant to facilitate comparison. We find that the number of detections is small regardless of the ice-mass fraction of the planets, similarly the number of potential detections is uniformly small, making a statistically significant null-result elusive. Irrespective of the red noise level, given our SNR detection threshold of 4.3σ, there were an average of 19 spurious false-positive 'transits' reported over each of the 2-year observing campaigns.

Transit detection from space has been a topic of discussion following the direct detection of HD 209458b by the Spizter Space Telescope (Deming et al., 2005), as well as the constraint on its albedo by the MOST telescope (Rowe et al., 2006). To examine the potential detection of our simulated planets using a dedicated space-based mission, we ran a simulation meant to emulate the general characteristics of the proposed TESS satellite. As before, we use our suite of planet-forming simulations to populate the target stars. The TESS satellite is designed to have six small ($\sim$ 13cm) wide-field cameras observing stars in the direction of the anti-solar point, with a total field of view of $\sim$ 2000 square degrees. This setup will yield $\sim$ 36 days of continuous photometry for each star over it's two year survey. Using a simplified version of our Monte-Carlo code, with a fixed exposure time of 1 minutes, we simulated observations of the 1385 best candidate stars in the LSPM-North catalog. This sample of stars was determined as described above but with the stellar size cut (TD_{crit}) based on the reduced noise level due to the lack of atmospheric scintillation. We then analyzed the resulting lightcurves by sliding a characteristic transit template along the lightcurve and for each time-alignment calculating a χ^2 value between the lightcurve and the template. We then divide this χ^2 value by the χ^2 of a null hypothesis (no transit). We fold this figure of merit time-sequence along the possible planetary periods, and search for periodic signals.

Of the 144 stars that had transits, 31 were clearly detectable while the rest are too small relative to the stellar (red) noise to be detected. If we assume that the Southern sky would allow another 31 detections and use an occurrence fraction of 28%, we find that such a mission would allow the detection of ~ 17 of the planets in our simulations after the two year survey.

5 Summary

It is generally agreed that if terrestrial planet formation around low-mass M-dwarfs is a scaled down version of solar system formation, then planets in the habitable zones of low-mass red dwarfs will be small, dry, and thoroughly inhospitable (see, e.g. Raymond et al., 2007; Lissauer, 2007). Nature, on the other hand, tends to defy expectations. Our tack here has been to investigate an alternative, optimistic scenario for terrestrial planet formation around nearby low mass stars, which assumes that disk-mass is largely independent of stellar mass. In this scenario, the planets that emerge are more akin to the Jovian satellites rather than Mercury, Venus, Earth and Mars. Our motivation for this investigation stems from the fact that our hypothesis is potentially testable, and at a relatively low cost.

Our approach couples end-to-end simulations of both the *in-situ* formation and the transit-detection of terrestrial mass planets around local, late-type M-dwarf stars. Our formation simulations followed the accretional growth of planetary embryos, around an $M_* = 0.12\,M_\odot$ star, from the onset of oligarchic growth ($M_{emb} \sim 3\times10^{21}$ g) using a semi-analytic method, through the stochastic late-phases of growth using a full 3-D Nbody simulation. These simulations resulted in systems of several (3-5) planets with masses comparable to Earth in stable orbits in or near the star's habitable zone as well as 1-2 planets per system with masses comparable to Mars. We found that these results were largely insensitive to the presence or absence of an exterior perturbing Neptune-mass planet, but detectable planets are more likely to occur if an external perturber is present.

Photometric red noise makes transit detection of these small planets challenging. We have explored the impact of varying levels of red noise on the potential utility of dedicated ground-based telescope arrays. Our method consisted of a detailed Monte-Carlo transit search code implementing realistic weather, stellar flux, telescope and M-dwarf noise models. We find that a formation frequency of $\sim 28\%$ and nightly stellar noise levels in the vicinity of $\sigma \sim 0.45$ mmag allow a longitudinally distributed array of ten dedicated meter-class telescopes carrying out a targeted search to detect, on average, 0.3 transiting terrestrial planets within two years of operation and another 0.5 potentially detectable planets. However, a satellite based survey similar to TESS is capable of detecting ~ 17 planets after it's two year survey.

Time and again over the past decade, nature has surprised planet hunters with the sheer diversity of planetary systems. Experience has shown that planet formation under a variety of conditions can be more efficient than the example of our own system would suggest. Our approach in this paper has been to investigate a planet building model that lies at the optimistic, yet still justifiable range of formation scenarios. Should our picture prove correct, then the prospects for discovery of truly earthlike, alarmingly nearby, and potentially habitable planets may lie close at hand.

Acknowledgements

This research has been supported by NSF CAREER Award AST-0449986, and by the NASA Origins of Solar Systems Program through grant NNG04GN30G. The authors wish to thank David Charbonneau and John Chambers for helpful discussions and technical advice concerning the `Mercury` code. Also thanks to Scott Seagroves and Justin Harker for the use of and advice concerning the `Transit-Search` code.

The IDL astronomy user's library is available at http://idlastro.gsfc.nasa.gov

References

Adachi, I., Hayashi, C., Nakazawa, K., Dec. 1976. The gas drag effect on the elliptical motion of a solid body in the primordial solar nebula. Progress of Theoretical Physics 56, 1756–1771.

Adams, E. R., Seager, S., Elkins-Tanton, L., Feb. 2008. Ocean Planet or Thick Atmosphere: On the Mass-Radius Relationship for Solid Exoplanets with Massive Atmospheres. ApJ673, 1160–1164.

Andrews, S. M., Williams, J. P., Dec. 2007. A Submillimeter View of Circumstellar Dust Disks in ρ Ophiuchi. ApJ671, 1800–1812.

Bayless, A. J., Orosz, J. A., Nov. 2006. 2MASS J05162881+2607387: A New Low-mass Double-lined Eclipsing Binary. ApJ651, 1155–1165.

Bennett, D. P., Feb. 2009. Detection of Extrasolar Planets by Gravitational Microlensing. ArXiv e-prints.

Bouchy, F., Pont, F., Melo, C., Santos, N. C., Mayor, M., Queloz, D., Udry, S., Mar. 2005. Doppler follow-up of OGLE transiting companions in the

Galactic bulge. A&A431, 1105–1121.

Butler, R. P., Vogt, S. S., Marcy, G. W., Fischer, D. A., Wright, J. T., Henry, G. W., Laughlin, G., Lissauer, J. J., Dec. 2004. A Neptune-Mass Planet Orbiting the Nearby M Dwarf GJ 436. ApJ617, 580–588.

Canup, R. M., Ward, W. R., Jun. 2006. A common mass scaling for satellite systems of gaseous planets. Nature441, 834–839.

Chambers, J., Feb. 2006. A semi-analytic model for oligarchic growth. Icarus 180, 496–513.

Chambers, J. E., Aug. 2001. Making More Terrestrial Planets. Icarus 152, 205–224.

Chambers, J. E., Migliorini, F., Jul. 1997. Mercury - A New Software Package for Orbital Integrations. Bulletin of the American Astronomical Society 29, 1024–+.

Chambers, J. E., Wetherill, G. W., Boss, A. P., Feb. 1996. The Stability of Multi-Planet Systems. Icarus 119, 261–268.

Delfosse, X., Forveille, T., Ségransan, D., Beuzit, J.-L., Udry, S., Perrier, C., Mayor, M., Dec. 2000. Accurate masses of very low mass stars. IV. Improved mass-luminosity relations. A&A364, 217–224.

Deming, D., Seager, S., Richardson, L. J., Harrington, J., Mar. 2005. Infrared radiation from an extrasolar planet. Nature434, 740–743.

Dravins, D., Lindegren, L., Mezey, E., Young, A. T., May 1998. Atmospheric Intensity Scintillation of Stars. III. Effects for Different Telescope Apertures. PASP110, 610–633.

Endl, M., Cochran, W. D., Kürster, M., Paulson, D. B., Wittenmyer, R. A., MacQueen, P. J., Tull, R. G., Sep. 2006. Exploring the Frequency of Close-in Jovian Planets around M Dwarfs. ApJ649, 436–443.

Gaidos, E., Haghighipour, N., Agol, E., Latham, D., Raymond, S., Rayner, J., Oct. 2007. New Worlds on the Horizon: Earth-Sized Planets Close to Other Stars. Science 318, 210–.

Gillon, M., Pont, F., Demory, B.-O., Mallmann, F., Mayor, M., Mazeh, T., Queloz, D., Shporer, A., Udry, S., Vuissoz, C., Sep. 2007. Detection of transits of the nearby hot Neptune GJ 436 b. A&A472, L13–L16.

Guedes, J. M., Rivera, E. J., Davis, E., Laughlin, G., Quintana, E. V., Fischer, D. A., Jun. 2008. Formation and Detectability of Terrestrial Planets around α Centauri B. ApJ679, 1582–1587.

Hauschildt, P. H., Allard, F., Baron, E., Feb. 1999. The NextGen Model Atmosphere Grid for $3000 \leq T_{eff} \leq 10,000$ K. ApJ512, 377–385.

Hubickyj, O., Bodenheimer, P., Lissauer, J. J., Dec. 2005. Accretion of the gaseous envelope of Jupiter around a 5 10 Earth-mass core. Icarus 179, 415–431.

Ida, S., Makino, J., Nov. 1993. Scattering of planetesimals by a protoplanet - Slowing down of runaway growth. Icarus 106, 210–+.

Kokubo, E., Ida, S., Sep. 1996. On Runaway Growth of Planetesimals. Icarus 123, 180–191.

Kokubo, E., Ida, S., Jan. 1998. Oligarchic Growth of Protoplanets. Icarus 131, 171–178.

Kokubo, E., Ida, S., Jan. 2000. Formation of Protoplanets from Planetesimals in the Solar Nebula. Icarus 143, 15–27.

Kokubo, E., Ida, S., Dec. 2002. Formation of Protoplanet Systems and Diversity of Planetary Systems. ApJ581, 666–680.

Laughlin, G., Bodenheimer, P., Adams, F. C., Sep. 2004. The Core Accretion Model Predicts Few Jovian-Mass Planets Orbiting Red Dwarfs. ApJ612, L73–L76.

Leggett, S. K., Allard, F., Dahn, C., Hauschildt, P. H., Kerr, T. H., Rayner, J., Jun. 2000. Spectral Energy Distributions for Disk and Halo M Dwarfs. ApJ535, 965–974.

Lépine, S., Oct. 2005. Nearby Stars from the LSPM-North Proper-Motion Catalog. I. Main-Sequence Dwarfs and Giants within 33 Parsecs of the Sun. AJ130, 1680–1692.

Lépine, S., Shara, M. M., Mar. 2005. A Catalog of Northern Stars with Annual Proper Motions Larger than 0.15" (LSPM-NORTH Catalog). AJ129, 1483–1522.

Levison, H. F., Agnor, C., May 2003. The Role of Giant Planets in Terrestrial Planet Formation. AJ125, 2692–2713.

Lissauer, J. J., 1993. Planet formation. ARA&A31, 129–174.

Lissauer, J. J., May 2007. Planets Formed in Habitable Zones of M Dwarf Stars Probably Are Deficient in Volatiles. ApJ660, L149–L152.

Lovis, C., Mayor, M., Pepe, F., Alibert, Y., Benz, W., Bouchy, F., Correia, A. C. M., Laskar, J., Mordasini, C., Queloz, D., Santos, N. C., Udry, S., Bertaux, J.-L., Sivan, J.-P., May 2006. An extrasolar planetary system with three Neptune-mass planets. Nature441, 305–309.

Lovis, C., Mayor, M., Pepe, F., Queloz, D., Udry, S., 2008. Pushing Down the Limits of the Radial Velocity Technique. In: Santos, N. C., Pasquini, L., Correia, A. C. M., Romaniello, M. (Eds.), Precision Spectroscopy in Astrophysics. pp. 181–184.

Mayor, M., Udry, S., Lovis, C., Pepe, F., Queloz, D., Benz, W., Bertaux, J. ., Bouchy, F., Mordasini, C., Segransan, D., Jun. 2008. The HARPS search for southern extra-solar planets. XIII. A planetary system with 3 Super-Earths (4.2, 6.9, and 9.2 Earth masses). ArXiv e-prints.

Nutzman, P., Charbonneau, D., Mar. 2008. Design Considerations for a Ground-Based Transit Search for Habitable Planets Orbiting M Dwarfs.

PASP120, 317–327.

O'Brien, D. P., Morbidelli, A., Levison, H. F., Sep. 2006. Terrestrial planet formation with strong dynamical friction. Icarus 184, 39–58.

Ohta, Y., Taruya, A., Suto, Y., Apr. 2005. The Rossiter-McLaughlin Effect and Analytic Radial Velocity Curves for Transiting Extrasolar Planetary Systems. ApJ622, 1118–1135.

Podolak, M., Zucker, S., Nov. 2004. A note on the snow line in protostellar accretion disks. Meteoritics and Planetary Science 39, 1859–1868.

Pollack, J. B., Hubickyj, O., Bodenheimer, P., Lissauer, J. J., Podolak, M., Greenzweig, Y., Nov. 1996. Formation of the Giant Planets by Concurrent Accretion of Solids and Gas. Icarus 124, 62–85.

Pont, F., Zucker, S., Queloz, D., Nov. 2006. The effect of red noise on planetary transit detection. MNRAS373, 231–242.

Quintana, E. V., Lissauer, J. J., Chambers, J. E., Duncan, M. J., Sep. 2002. Terrestrial Planet Formation in the α Centauri System. ApJ576, 982–996.

Raymond, S. N., Barnes, R., Mandell, A. M., Feb. 2008. Observable consequences of planet formation models in systems with close-in terrestrial planets. MNRAS384, 663–674.

Raymond, S. N., Quinn, T., Lunine, J. I., Mar. 2004. Making other earths: dynamical simulations of terrestrial planet formation and water delivery. Icarus 168, 1–17.

Raymond, S. N., Scalo, J., Meadows, V. S., Nov. 2007. A Decreased Probability of Habitable Planet Formation around Low-Mass Stars. ApJ669, 606–614.

Rivera, E. J., Lissauer, J. J., Butler, R. P., Marcy, G. W., Vogt, S. S., Fischer, D. A., Brown, T. M., Laughlin, G., Henry, G. W., Nov. 2005. A $\sim 7.5 M_\oplus$ Planet Orbiting the Nearby Star, GJ 876. ApJ634, 625–640.

Rockenfeller, B., Bailer-Jones, C. A. L., Mundt, R., Mar. 2006. Variability and periodicity of field M dwarfs revealed by multichannel monitoring. A&A448, 1111–1124.

Rowe, J. F., Matthews, J. M., Seager, S., Kuschnig, R., Guenther, D. B., Moffat, A. F. J., Rucinski, S. M., Sasselov, D., Walker, G. A. H., Weiss, W. W., Aug. 2006. An Upper Limit on the Albedo of HD 209458b: Direct Imaging Photometry with the MOST Satellite. ApJ646, 1241–1251.

Safronov, V. S., 1969. Evolution of the protoplanetary cloud and formation of the earth and the planets, nasa ttf-677 Edition. Jerusalem, Israel Program for Scientific Translations, 1972.

Seagroves, S., Harker, J., Laughlin, G., Lacy, J., Castellano, T., Dec. 2003. Detection of Intermediate-Period Transiting Planets with a Network of Small Telescopes: transitsearch.org. PASP115, 1355–1362.

Selsis, F., Kasting, J. F., Levrard, B., Paillet, J., Ribas, I., Delfosse, X., Dec. 2007. Habitable planets around the star Gliese 581? A&A476, 1373–1387.

Thébault, P., Marzari, F., Scholl, H., Aug. 2008. Planet formation in α Centauri A revisited: not so accretion friendly after all. MNRAS388, 1528–1536.

Thébault, P., Marzari, F., Scholl, H., Feb. 2009. Planet formation in the habitable zone of α Centauri B. MNRAS393, L21–L25.

Valencia, D., Sasselov, D. D., O'Connell, R. J., Aug. 2007. Detailed Models of Super-Earths: How Well Can We Infer Bulk Properties? ApJ665, 1413–1420.

Weidenschilling, S. J., Sep. 1977. The distribution of mass in the planetary system and solar nebula. Ap&SS51, 153–158.

Weidenschilling, S. J., Spaute, D., Davis, D. R., Marzari, F., Ohtsuki, K., Aug. 1997. Accretional Evolution of a Planetesimal Swarm. Icarus 128, 429–455.

Wetherill, G. W., Stewart, G. R., Feb. 1989. Accumulation of a swarm of small planetesimals. Icarus 77, 330–357.

Wetherill, G. W., Stewart, G. R., Nov. 1993. Formation of planetary embryos

- Effects of fragmentation, low relative velocity, and independent variation of eccentricity and inclination. Icarus 106, 190–+.

Final Planetary Configuration Statistics

Simulation Group		$\overline{N}_{Planet}$	$\overline{M}_{Planet}$	Mass Lost	$\overline{N}_p$
A	No Ice-giant	4.4	0.79	2%	1.4
B	Ice-giant present	3.8	0.68	18%	0.2

Table 1

"Planet" indicates masses above $0.05 M_{\oplus}$. $\overline{N}_{Planet}$ is the average number of planets per system. $\overline{M}_{Planet}$ is the median mass of planets per system. $\overline{N}_p$ is the average number of planetary embryos that survived per system.

Comparison of Planetary Compositions, Radii and Detectability

Ice	$\overline{R}_p$	$\overline{N}_{detect}$	$\overline{N}_{possible}$
100%	1.46	0.4	0.6
50%	1.20	0.3	0.5
0%	0.93	0.1	0.3
50%*	0.68	0.1	0.1
50%**	0.24	0.0	0.0

Table 2

Columns indicate the planetary ice-mass-fraction (Valencia et al., 2007), median resulting planetary radius (in Earth radii), the number of planets detected in our observing scenario after the two year simulated observing campaign, and the number of additional planets potentially detectable given the levels of rednoise present, respectively. Assuming an occurrence fraction of 28%.

The bottom two rows respresent our low disk-mass simulations with normalizations of * $7\,\mathrm{g/cm^2}$ and ** $0.84\,\mathrm{g/cm^2}$.

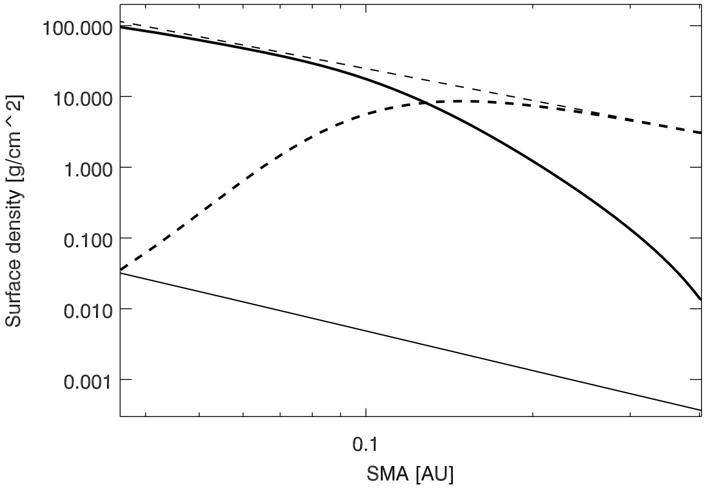

Fig. 1. Beginning/end (thin/thick lines) surface density profiles of the planetary embryos and planetesimals (solid and dashed lines, respectively) from the semi-analytic model. The semi-analytic model runs until ~ 150 years.

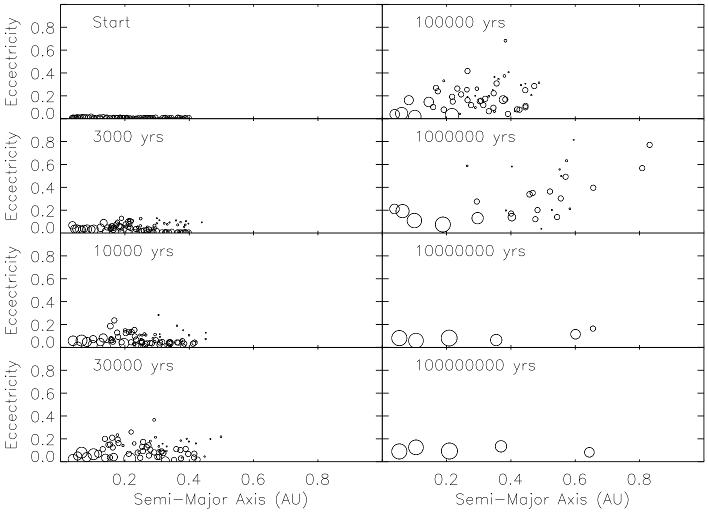

Fig. 2. Evolution of Simulation A-01 (no ice-giant present) ending with planets of mass 0.86, 0.79, 1.03, 0.36 and 0.22 $M_{\oplus}$ (in order of increasing semi-major axis) after 10^8 years. The size of the symbol is proportional to the radius of the body.

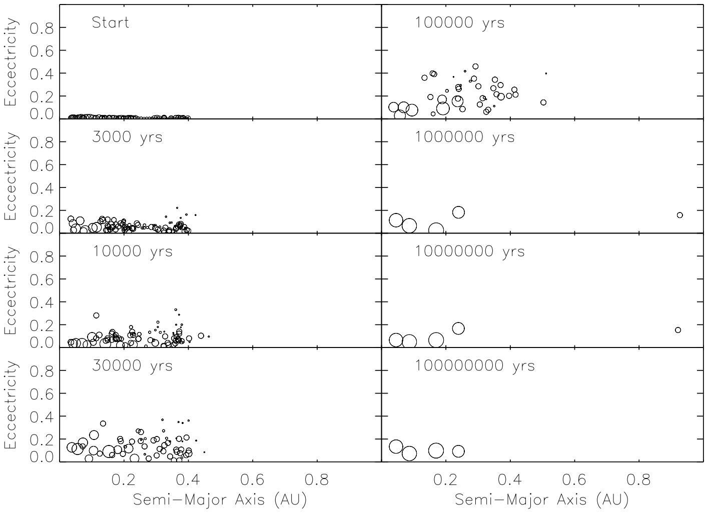

Fig. 3. Evolution of Simulation B-01 (ice-giant at 0.6AU) ending with planets of mass 0.60, 0.75, 0.83, and 0.41 $M_\oplus$ (in order of increasing semi-major axis) after 10^8 years. The size of the symbol is proportional to the radius of the body.

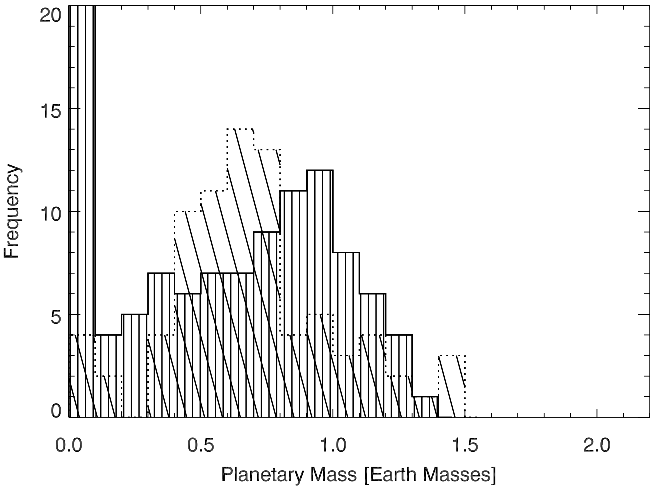

Fig. 4. Final planet masses using a non-uniform initial mass distribution. Group A is represented by the solid line (no ice-giant present). Group B is represented by the dotted line (ice-giant at 0.6AU).

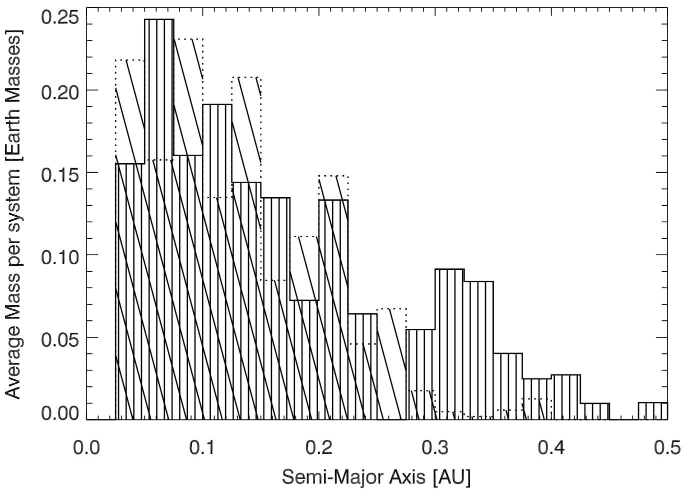

Fig. 5. The amount of mass located in each semi-major axis bin. Group A is represented by the solid line (no ice-giant present). Group B is represented by the dotted line (ice-giant at 0.6AU).

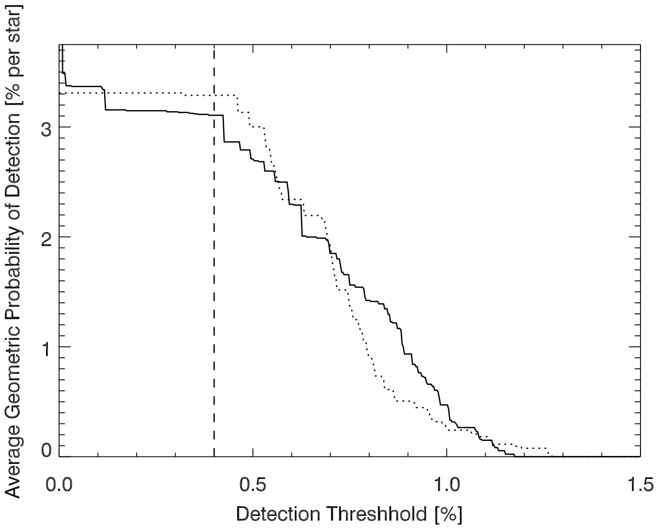

Fig. 6. Probability of detecting a transit of a planet around its host star as a function of the telescope's sensitivity. Dotted line shows the simulations with an ice-giant, solid line shows the simulations without. An approximate sensitivity of sub-meter class telescopes is shown for comparison ($\sim$ 3 milli-magnitudes).

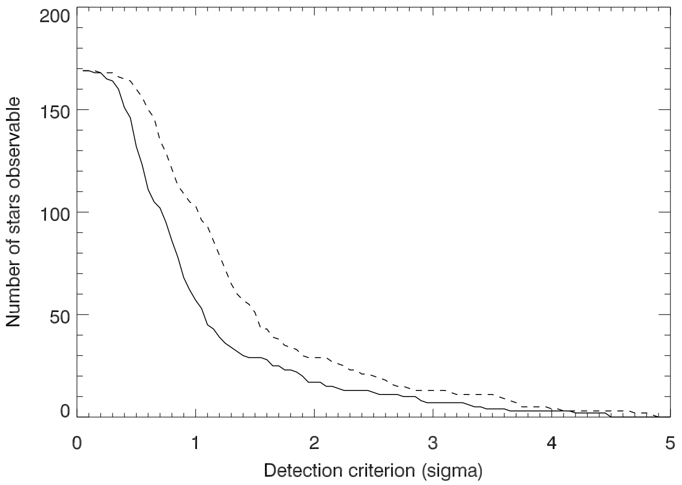

Fig. 7. Number of stars which could yield detectable transit signals in a 20 (30) minute exposure as a function of signal-to-noise requirement, shown by the solid (dashed) line.

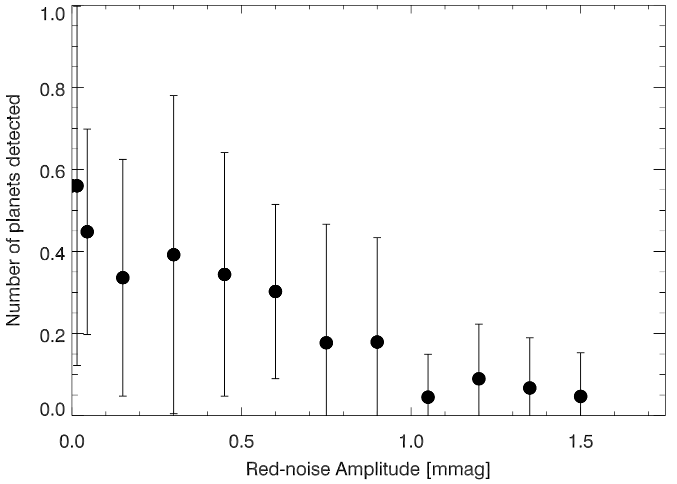

Fig. 8. Number of transit detection after two years of observation by a dedicated array of meter-class telescopes, as a function of red noise amplitude. Scaled to an occurence fraction of 28%.